Strong four-photon conversion regime of cross-phase-modulation-induced modulational instability

Emmanuel Seve and Guy Millot
Laboratoire de Physique de l'Université de Bourgogne, Faculté des Sciences Mirande, 9 Avenue A. Savary, Boîte Postale 47 870, 21078 Dijon, France

Stefano Trillo
Dipartimento di Ingegneria, University of Ferrara, Via Saragat 1, 44100 Ferrara, Italy
(Received 7 July 1999; revised manuscript received 1 November 1999)

We investigate theoretically and experimentally the strong conversion regime of parametric four-photon amplification or induced modulational instability in the normal dispersion regime of propagation in a highly birefringent fiber. Such optical mixing is observed by injecting a tunable linearly polarized (along the fast axis) anti-Stokes signal wave copropagating with a pump equisplitted between the fiber axes (i.e., linearly polarized at 45°) which entail that the two pump modes experience cross-phase modulation. In agreement with a four-wave model developed to study the *depleted* regime of the mixing process, we observe that the strongest conversion occurs outside the parametric gain bandwidth, or in other words, under conditions of *modulational stability* of the pump beam. This proves that the optimum signal frequency deviates significantly from the prediction of the linear stability analysis or the usual phase-matching argument.

PACS number(s): 41.20.Jb, 47.20.−k, 42.65.Sf, 52.35.Mw

I. INTRODUCTION

Optical fibers are now widely used to test general concepts of nonlinear wave dynamics such as soliton and modulational instabilities. In this sense they provide a unique testbed of the validity of predictions based on nonlinear propagation models directly derived from Maxwell equations complemented by the nonlinear constitutive relations. Among the striking phenomena due to the interplay of the dispersive and Kerr effects is the modulational instability (MI), entailing the exponential growth of a perturbation with long-wavelength at the expense of a cw pump [1–8]. The amplified perturbation can be either quantum noise (i.e., spontaneous MI [6]) or a frequency shifted signal wave (i.e., induced MI [7]). In the frequency domain, MI is equivalent to a four-photon mixing process where two pump photons (ω_p) are anihilated to create a Stokes ($\omega_S=\omega_p-\Omega$)–anti-Stokes ($\omega_a=\omega_p+\Omega$) photon pair, with the energy conservation rule $2\omega_p=\omega_S+\omega_a$. In the scalar case, the momentum conservation $2k_p=k_S+k_a$ can be fulfilled only in the anomalous group-velocity dispersion (GVD) regime (usually for $\lambda>1.3\,\mu$m), thanks to the intensity-dependent refractive index contributions. Remarkably, however, MI occurs also with normal GVD, thanks to the coupling between two modes of the e.m. field [9–25]. Different coupling arrangements involve two polarization modes, two different pump wavelengths, or two higher-order modes. Except for the low-birefringence fiber [11,15,19], where the pump polarization might have a nonlinear rotation and the pump components are generally allowed to exchange energy [24], all the other mentioned MI processes are sustained by cross-phase modulation. This means that the pump power is distributed between two modes of the e.m. field which experience only mutual nonlinear phase changes without exchanging energy (the transfer of energy only occurs between the two pump modes and the new generated or amplified sideband frequencies). The high-birefringence fiber seems, however, the most convenient setting for investigating a MI process induced genuinely by cross-phase modulation, since it does not suffer the drawback of competing four-wave processes as in the dual-wavelength pumping case [12], and the control of the pump mode-balance is simpler than the case of pumping higher order modes [23].

The question which we address here, concerns the development of MI beyond the initial stage of exponential growth, or in other word the strong conversion regime of parametric amplification. It has been recently shown that, in the time domain, MI in the normal GVD leads to the formation of terahertz trains of dark solitons or polarization domain walls, which can be eventually recurrent along the propagation [25–27]. The shape of the temporal structures depends on the powers of the different waves and the modulational frequency [26]. In the frequency domain, this pulse generation via MI manifests itself by the growing of a cascade of sidebands. The number of harmonics is related to the temporal shape of the generated pulses, in turn fixed by the input conditions [26].

Here, we are rather concerned with the interaction of a single sideband pair (a four-wave interaction) which occurs for a narrowband MI process such as that taking place in a highly birefringent fiber at moderately low power. We specifically address the problem of determining the signal frequency detuning which, in an experiment of induced MI, permits us to achieve the strongest parametric amplification.

Theoretically, the answer to this question requires to account for pump depletion, or in other words to construct a theory of nonlinear MI. This can be conveniently done by using a standard approach employed for both dissipative [28], and conservative models [29], which consists to reduce the original model to a system of coupled ordinary differential equations (ODEs) for the Fourier mode amplitudes which drive the dynamics. This is particularly useful for non-

integrable (from the point of view of the spectral transform method) models such as the one we will deal with, where other methods (see, e.g., Ref. [30], and references therein) to construct exact periodic spatiotemporal solutions cannot be easily applied. This approach has proved useful to describe conservative nonlinear MI in the scalar case [31,32], in the low birefringence fiber [33–35], as well as cross-phase modulation induced MI [36,37]. The main outcome of the theory is the existence of a homoclinic structure of the governing models, whose main signature is the fact that strong conversion can be achieved outside the parametric MI gain bandwidth of the process (for narrowband MI), or in other words in a regime of *modulational stability* of the pump mode. This is made possible by the existence of a new regime of instability, where the unstable mode which sustains the mixing is no longer the pump, but a mixed pump-sideband mode [36,37].

Experimentally, it has recently been demonstrated that the strong conversion regime is indeed observable in experiments with relatively short fibers in order to avoid stimulated Raman scattering [38–41]. Careful measurements in a low birefringence fiber has confirmed the theoretical predictions [38–40]. Here we show that the strong conversion regime is accessible with relatively low powers also in a high-birefringence fiber under quasi-cw conditions (i.e., with nanosecond pulses). The experimental results confirm that the highest conversion is achieved at a signal frequency significantly different from that corresponding to the peak MI gain or nonlinear phase-matching frequency.

This paper is organized as follows. In Sec. II, we introduce the nonlinear Schrödinger model which governs the interaction. We recall the basic results about MI, analyze the unidimensional oscillator based on the Fourier mode truncation of the original model, and comment on its validity. Section III is devoted to the presentation of the experimental results concerning the mixing. Finally, we present our conclusions in Sec. IV.

II. THEORY

A. Coupled nonlinear Schrödinger equations

In a highly birefringent optical fiber, the propagation of a quasimonochromatic field $E(\mathbf{r},Z,T)=[E_x(Z,T)\exp(ik_xZ)+E_y(Z,T)\exp(ik_yZ)]f(\mathbf{r})\exp(-i\omega_0 t)$, with arbitrary polarization is governed by a set of two incoherently coupled nonlinear Schrödinger equations (ICNLSEs) [13–15,21,37]

$$\frac{\partial E_x}{\partial Z}+\frac{1}{V_x}\frac{\partial E_x}{\partial T}+i\frac{k''}{2}\frac{\partial^2 E_x}{\partial T^2}=i\gamma(|E_x|^2+r|E_y|^2)E_x,$$
$$\frac{\partial E_y}{\partial Z}+\frac{1}{V_y}\frac{\partial E_y}{\partial T}+i\frac{k''}{2}\frac{\partial^2 E_y}{\partial T^2}=i\gamma(|E_y|^2+r|E_x|^2)E_y, \tag{1}$$

where E_x and E_y are the slowly varying amplitudes of the linearly polarized components along the slow and fast axis, respectively, $V_{x,y}$ are their group velocities, and k'' is the group-velocity dispersion (assumed isotropic). Here $\gamma=2\pi n_2/(\lambda_p A_{\rm eff})$ is the standard nonlinear coefficient, and r stands for the cross to parallel susceptibility ratio ($r=\frac{2}{3}$ in silica fibers). All these coefficients are evaluated at the pump wavelength λ_p. Since the fiber length ($Z\simeq 2$ m) used in our experiments is relatively short, the effect of losses and Raman scattering can be reasonably neglected and we do not include them in Eqs. (1). Hence we are left with the effect of the anisotropic dispersion [left-hand sides of Eqs. (1)], and the fast Kerr nonlinearity which induces self-phase and cross-phase modulations. The nonlinear coherent coupling terms (see, e.g., Ref. [40]), which governs the energy exchange between the fiber modes have been dropped owing to their fast oscillation during the propagation.

For the sake of comparison between the field dynamics ruled by ICNLSEs and the four-wave truncated evolution, we will make use of the following normalized version of Eqs. (1):

$$i\frac{\partial u_x}{\partial z}+i\delta\frac{\partial u_x}{\partial t}-\frac{\beta}{2}\frac{\partial^2 u_x}{\partial t^2}+(|u_x|^2+r|u_y|^2)u_x=0,$$
$$i\frac{\partial u_y}{\partial z}-i\delta\frac{\partial u_y}{\partial t}-\frac{\beta}{2}\frac{\partial^2 u_y}{\partial t^2}+(|u_y|^2+r|u_x|^2)u_y=0, \tag{2}$$

where $u_{x,y}\equiv E_{x,y}/\sqrt{P_{\rm tot}}$, $z\equiv Z/Z_{nl}$, $t\equiv(T-Z/V)T_0^{-1}$ stands for a retarded time in a frame traveling at the average group-velocity $V=[\frac{1}{2}(V_x^{-1}+V_y^{-1})]^{-1}$, $Z_{nl}=(\gamma P_{\rm tot})^{-1}$ and $T_0=\sqrt{|k''|Z_{nl}}$ being the characteristic length and time scales associated with the total (conserved) input power $P_{\rm tot}=|E_x|^2+|E_y|^2$, respectively. Here $\delta=\frac{1}{2}T_0(V_x^{-1}-V_y^{-1})/|k''|$ is a normalized walk-off parameter (note that it depends inversely on the square root of total power through T_0), and $\beta=\mathrm{sgn}(k'')$.

It is well known that any cw eigensolution of Eqs. (1) with components $E_x=E_{x0}=\sqrt{P_x}\exp(i\phi_x)$ and $E_y=E_{y0}=\sqrt{P_y}\exp(i\phi_y)$, and phases $\phi_{x,y}=(P_{x,y}+rP_{y,x})Z$, is modulationally unstable [13–15,21,37], that is, starting from the ansatz $E_j=[E_{j0}+E_{ja}\exp(-i2\pi fT)+E_{js}\exp(i2\pi fT)]\exp(i\phi_j)$, $j=x,y$, the standard linear stability analysis (LSA) implying $E_{ja,js}\ll E_{j0}$, yields a linearized problem for the perturbation vector $[E_{xa},E_{xs}^*,E_{ya},E_{ys}^*]^T$ with real positive eigenvalues λ which in turn correspond to a parametric gain $G=2\,\mathrm{Re}(\lambda)$ in a proper range of the frequency detuning f. The outcome of the analysis is summarized in Fig. 1 which shows the normalized gain $g=GZ_{nl}$ versus the dimensionless modulational frequency $\Omega=2\pi fT_0$, and the normalized walk-off parameter δ, either in the normal [Figs. 1(a) and 1(b)], or in the anomalous [Figs. 1(c) and 1(d)] GVD regime, for a beam with $P_x=P_y$ (i.e., linearly polarized at 45°). The contour lines of g in Figs. 1(b) and 1(d) clearly show the domains of MI. In particular, the low-frequency branch in Figs. 1(c) and 1(d) is associated with the usual scalar MI. Our experiment is aimed, instead, at studying the polarization MI associated with the high-frequency branch. Therefore, in the anomalous GVD regime, even when the latter MI process is probed with an appropriate choice of frequency and polarization seed, we expect that a spontaneous MI at low frequency could compete and hamper the effects that we are seeking for. For this reason, henceforth we will focus only on the normal GVD regime. In order to show that one can tune the MI gain curve along the δ axis in Figs. 1(a) and 1(b) simply by changing the total

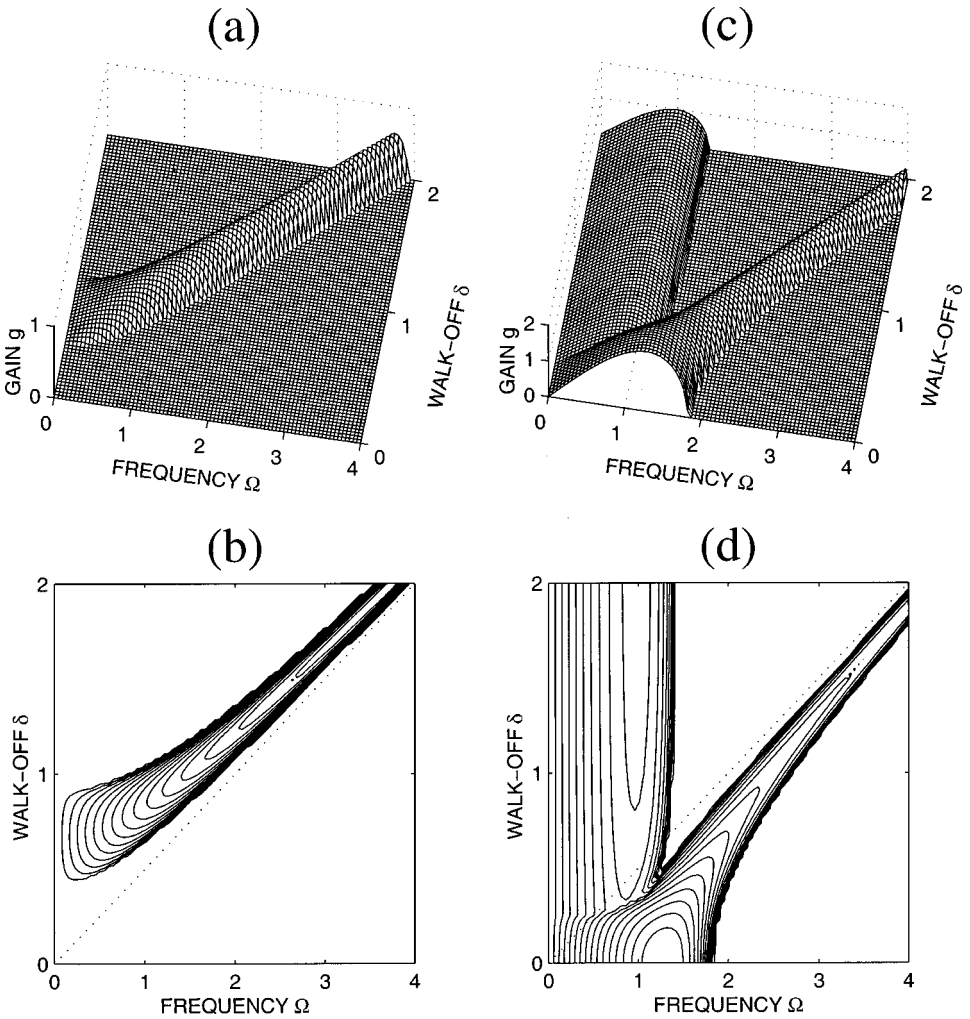

FIG. 1. MI gain $g=g(\Omega,\delta)$ as a function of the normalized frequency detuning Ω and walk-off parameter δ: (a) and (b), normal GVD regime; (c) and (d), anomalous GVD regime. The dashed line in (b) and (d) corresponds to the linear phase matching.

power, we show in Fig. 2 the dimensional spectral gain $G=G(f)$ which corresponds to our experimental parameters (see below) with a total pump peak power $P_p=P_x+P_y=56\,\mathrm{W}$ (dashed curve), 112 W (solid curve), and 160 W (dot-dashed curve). We emphasize that, in general, the exponentially growing mode associated with the narrowband MI of Figs. 1(a) and 1(b), has *all the four* sideband components. However, for large enough δ (i.e., relatively low powers) only two components survive, namely, the Stokes and anti-Stokes polarized along the slow and fast axis, respectively [15,37]. This can be shown, e.g., by analyzing the fractional wave content of the eigenvector corresponding to the unstable eigenvalue in the LSA [15], and it is supported by several experimental observations. In this case it is generally expected that the most simple and effective way to stimulate MI is by means of a copropagating signal beam, polarized along the fast (slow) axis, with optimum anti-Stokes (Stokes) frequency detuning from the pump frequency. Here, in the spirit of the LSA, optimum indicates the peak gain detuning in the curves shown in Figs. 1 and 2. The narrow bandwidth of the process entails that the higher harmonics of the signal and the generated idler fall outside the parametric gain bandwidth and hence are not amplified. However, if the fiber is long enough the conversion towards the signal-idler sideband pair can be so strong that the undepleted-pump approximation implicit in the LSA is no longer valid. Under these conditions, the propagation past the early stage of exponential amplification must be treated by retaining the pump depletion in an exactly solvable model which takes into account the minimum number of effective modes [37]. The question which we specifically address is whether the optimum MI frequency still yields the largest amplification in the depleted stage of propagation.

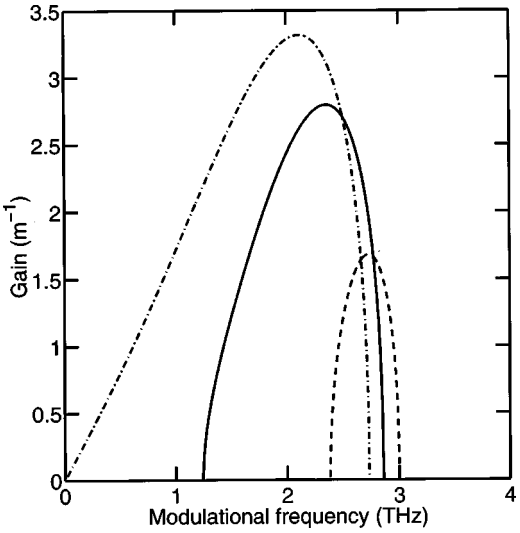

FIG. 2. MI gain G spectral profiles for a pump wave polarized at 45° between the fiber axes with total pump peak power $P_p=56\,\mathrm{W}$ (dashed), 112 W (solid), and 160 W (dot-dashed).

B. Four-mode truncation and phase matching

The dynamics of parametric amplification beyond the undepleted stage of propagation can be investigated by means of a truncated Fourier expansion of the envelopes $u_{x,y}$ in the ICNLSE [Eq. (2)]. Our analysis follows the approach of Refs. [36,37]. There are, however, important extensions to be made in order to describe the experimental results, since the results of Refs. [36,37] are limited to the phase-dependent dynamics of symmetric sidebands, whereas the experiment is carried out with strongly asymmetric input (i.e., a vanishing idler wave). We begin by expanding the two normalized field envelopes in Eqs. (2) as

$$u_j(z,t)=\sum_{n=-N}^{N} u_{j,n}(z)e^{-i\,n\Omega\,t};\quad j=x,y. \tag{3}$$

In principle one can obtain a self-consistent system of ODEs for an arbitrary number of sideband modes in Eq. (3). However, in practice, the approach turns out to be useful whenever the number of effective degrees of freedom of the reduced system is low enough. In the high-birefringence fiber, the six-wave mixing of the linearly polarized pump beams with the four first-order polarized sidebands is already sufficient to favor the onset of spatial chaos [37]. Importantly enough, however, if the walk-off is relatively high, only one pair of sidebands is effective (the Stokes and anti-Stokes sidebands are polarized along the slow and fast axes). As a consequence, we consider the evolution equations for the pump $[u_{px,y}(z)=E_{px,y}(z)/P_{\rm tot}]$, Stokes $[u_S(z)=E_S(z)/P_{\rm tot}]$, and antiStokes $[u_a(z)=E_a(z)/P_{\rm tot}]$ complex amplitudes, obtained by inserting in the ICNLSE (2), the fields $u_x(z,t)=u_{px}(z)+u_S(z)\exp(i\Omega t)$, $u_y(z,t)=u_{py}(z)+u_a(z)\exp(-i\Omega t)$. We obtain

$$-i\frac{du_{px}}{dz}=[|u_{px}|^2+r|u_{py}|^2+2|u_S|^2+r|u_a|^2]u_{px}+r\,u_S u_a u_{py}^*$$

$$=\frac{\partial H}{\partial u_{px}^*},\tag{4}$$

$$-i\frac{du_{py}}{dz}=[|u_{py}|^2+r|u_{px}|^2+2|u_a|^2+r|u_S|^2]u_{py}+r\,u_S u_a u_{px}^*$$

$$=\frac{\partial H}{\partial u_{py}^*},$$

$$-i\frac{du_S}{dz}=\left[\frac{\kappa}{2}+2|u_{px}|^2+r|u_{py}|^2+|u_S|^2+r|u_a|^2\right]u_S$$

$$+ru_{px}u_{py}u_a^*=\frac{\partial H}{\partial u_S^*},$$

$$-i\frac{du_a}{dz}=\left[\frac{\kappa}{2}+2|u_{py}|^2+r|u_{px}|^2+|u_a|^2+r|u_S|^2\right]u_a$$

$$+ru_{px}u_{py}u_S^*=\frac{\partial H}{\partial u_a^*},$$

where the Hamiltonian reads

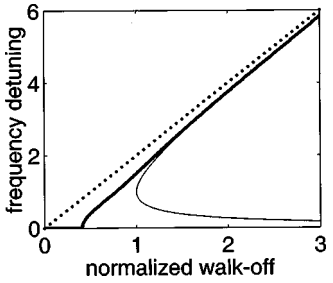

FIG. 3. Comparison between the optimum MI frequency detuning (thick solid curve), the nonlinear phase-matching curve $\kappa=-1$ (thin solid line), and the linear phase-matching frequency (dashed line) versus the normalized walk-off δ.

$$H=\frac{\kappa}{2}(|u_a|^2+|u_S|^2)+\sum_j\frac{|u_j|^4}{2}+ru_{px}u_{py}u_S^*u_a^*+\text{c.c.}$$

$$+2(|u_{px}u_S|^2+|u_{py}u_a|^2)+r(|u_{px}u_a|^2+|u_{py}u_S|^2) \tag{5}$$

and we have introduced the parameter

$$\kappa\equiv\beta\Omega^2-2\,\delta\Omega=\frac{2\pi}{\gamma P_{\rm tot}}\left[2\pi k''f^2-\left(\frac{1}{V_x}-\frac{1}{V_y}\right)f\right]. \tag{6}$$

Here $\kappa\equiv\Delta k/(\gamma P_{\rm tot})$, with $\Delta k=k_S+k_a-k_{px}-k_{py}$, represents a normalized wave vector mismatch, and Eq. (6) follows immediately from the second-order expansion of k_j $(j=a,S,px,py)$ consistently with the validity of the ICNLSE model (1)–(2). Linear (i.e., low-power) phase-matching, occurs for $\kappa=0$ or $\Omega=2\,\delta$. However, the maximum conversion in the undepleted pump approximation occurs when the phase-matching generalized to include the nonlinear refractive index contributions, usually known as the *nonlinear* phase-matching condition, is fulfiled [37]. This can be easily seen from the linearized (i.e., $|u_{a,S}|\ll|u_{px,py}|$) version of the four-wave Eqs. (4) which, in terms of new variables $\overline{u_s}(z)=u_S(z)\exp[i(\kappa/2+2p_x+p_y)z]$ and $\overline{u_a}(z)=u_a(z)\exp[i(\kappa/2+2p_y+p_x)z]$, read as

$$u_{px}(z)=\sqrt{p_x}e^{i(p_x+rp_y)z},\quad u_{py}(z)=\sqrt{p_y}e^{(p_y+rp_x)z},$$

$$-i\frac{d\overline{u_S}}{dz}=r\sqrt{p_xp_y}\overline{u_a^*}e^{-i(\kappa+p_x+p_y)z},$$

$$i\frac{d\overline{u_a^*}}{dz}=r\sqrt{p_xp_y}\overline{u_S}e^{i(\kappa+p_x+p_y)z}, \tag{7}$$

where $p_{x,y}=|u_{px,py}|^2$ are constant pump power fractions $(p_x+p_y=1)$. From Eqs. (7) it is clear that the pump modes experience only cross-phase modulation while the maximum flow of energy to the sidebands occurs for a vanishing exponent $\kappa+p_x+p_y=0$, which is nothing but the nonlinear phase matching condition $\kappa=-(p_x+p_y)=-1$. In Fig. 3 we compare the nonlinear phase matching curve with the optimum MI frequency obtained from the six-wave LSA outlined above. As shown the two curves deviates significantly when the normalized walk-off decreases below $\delta\simeq1$ where the effect of the other Stokes–anti-Stokes pair becomes no longer negligible. At large values of δ (i.e., low power) the

nonlinear phase-matching approaches the linear one, as required on the physical ground.

Let us consider the regime of intermediate powers (as employed in the experiment) where the six-wave LSA and the nonlinear phase-matching condition give consistent results (see Fig. 3). Here we present a physical argument explaining why, in the presence of pump depletion, we expect stronger conversions to occur at larger signal detuning than the optimum one (this qualitative argument will be supported by quantitative rigorous results in the next subsection). We know that the optimum or nonlinear phase-matching frequency increases with decreasing pump power (see also Fig. 2). Therefore the effect of a progressive (i.e., locally along the fiber) pump depletion is that of increasing progressively the phase-matching frequency. As a consequence a signal at frequency lower or equal to the phase-matching frequency will be progressively driven out of phase-matching, and hence its conversion rate will eventually decrease. Viceversa, a signal with frequency higher than the phase-matching frequency will be pushed toward phase-matching by the effect of pump depletion, thereby leading to an overall higher conversion. Following this naive picture, a mixing enhancement can be generally expected even if the signal frequency falls outside the parametric gain bandwidth on the high-frequency edge. We will show below that this is indeed the case, the mixing process being sustained by an unstable mode which is no longer the pump but a mixed four-wave mode. Incidentally we recall that in a low-birefringence fiber, the same physical argument leads to conclude that the behavior is just opposite. Conversion enhancement takes place on the low-frequency side with a maximum outside the linear gain bandwidth [38–40]. The reason of this opposite frequency offset comes from the fact that the nonlinear phase-matching frequency increases with pump power in the weakly birefringent fiber [11].

C. Integrable strong-conversion dynamics

Let us proceed to reduce further the truncated four-wave mixing system (4) by exploiting the invariance or conservation laws which arise from fundamental principles. The Manley-Rowe relations imply the invariance of the quantities $P_{dp}=|E_{py}|^2-|E_{px}|^2$ and $P_{dS}=|E_a|^2-|E_S|^2$, which entail that photons are converted in pairs from the pump beams to the detuned Stokes–anti-Stokes sidebands. Whereas the absence of losses implies the conservation of the total power $P_{\rm tot}=|E_{py}|^2+|E_{px}|^2+|E_a|^2+|E_S|^2$. Following the approach of Refs. [31–37], we reduce the four-wave mixing equations to a one-dimensional equivalent Hamiltonian oscillator with two z-dependent variables playing the role of action-angle canonical variables: the single pump intensity fraction $\eta(z)=|E_{px}(z)|^2/P_{\rm tot}$ and the effective phase $\phi(z)=\phi_s(z)+\phi_a(z)-\phi_{px}(z)-\phi_{py}(z)$, where $\phi_j(z)$ is the phase of each individual wave u_j, $j=px$, py, a, S. These variables obey the system

$$\frac{d\eta}{dz}=\frac{\partial H}{\partial\phi};\quad \frac{d\phi}{dz}=-\frac{\partial H}{\partial\eta}, \tag{8}$$

$$H=r\sqrt{\eta(\eta+\alpha_p)[(1-2\eta-\alpha_p)^2-\alpha^2]}\cos\phi -(\kappa-1)\eta-\eta^2, \tag{9}$$

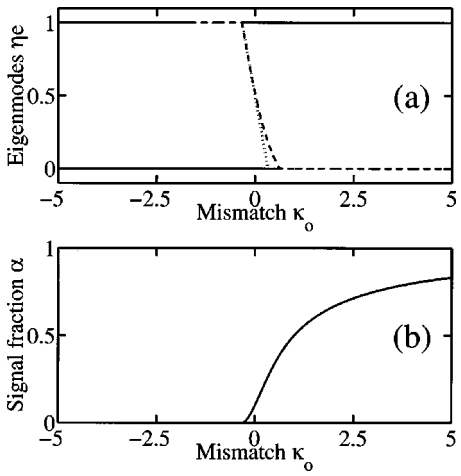

FIG. 4. (a) Solid (dashed) curves, fractional pump power η_e of the spatially stable (unstable) eigenmodes versus the normalized mismatch κ_0; (b) dependence of the critical signal fractional power $\alpha=\alpha_c$ on mismatch κ_0.

where the fractional Manley-Rowe invariants $\alpha=P_{dS}/P_{\rm tot}$ and $\alpha_p=P_{dp}/P_{\rm tot}$ play the role of parameters which are specified univocally by the initial conditions. In particular, α_p accounts for the pump unbalance: for sake of simplicity, we will consider only the case of a balanced pump beam polarized at 45° between the birefringence axes. This is indeed the case which yields the maximum amplification. In this case, the Hamiltonian oscillator (8),(9), by setting $\alpha_p=0$ and $\eta\to 2\eta$ (so that η is the total power fraction), reduces to the standard form Hamiltonian system [40]

$$\frac{d\eta}{dz}=\frac{\partial H}{\partial\phi}=-r\eta\sqrt{(1-\eta)^2-\alpha^2}\sin\phi, \tag{10}$$

$$\frac{d\phi}{dz}=-\frac{\partial H}{\partial\eta}=\kappa-1+2\eta-r\frac{1+2\eta^2-3\eta-\alpha^2}{\sqrt{(1-\eta)^2-\alpha^2}}\cos\phi, \tag{11}$$

$$H=r\eta\sqrt{(1-\eta)^2-\alpha^2}\cos\phi-(\kappa-1)\eta-\eta^2. \tag{12}$$

In our experiment, only one sideband is injected in the fiber (i.e., the anti-Stokes), and hence the initial condition is fixed to be $\eta_0=\eta(z=0)=1-\alpha$. Moreover, to compare sets of data obtained for constant pump power, we find convenient to introduce the mismatch parameter $\kappa_0=\Delta k/(\gamma P_p)=\kappa P_{\rm tot}/P_p=\kappa/(1-\alpha)$. The four-wave parametric conversion turns out to be dramatically affected by those eigenmodes of the process [the invariant solutions $\eta=\eta_e,\phi=\phi_e$ of Eqs. (10)–(12)] which are unstable. A detailed derivation of these eigenmodes is provided in the Appendix. Figure 4 summarizes the results. In Fig. 4(a) we show the fractional pump power η_e versus κ_0 of all the relevant stable and unstable eigenmodes as solid and dashed curves, respectively. The instability range $-\frac{5}{3}<\kappa_0<-\frac{1}{3}$ of the pump mode ($\eta_e=1$, obtained in the limit $\alpha=0$) corresponds to MI in the usual undepleted pump approximation [33,37]. The midvalue $\kappa_0=-1$ realizes the nonlinear phase matching of the four-wave parametric process. At $\kappa_0=-\frac{1}{3}$ the pump wave becomes stable, exchanging its stability with a new bifurcating mixed-mode eigensolution (a mixture of phase-locked pump

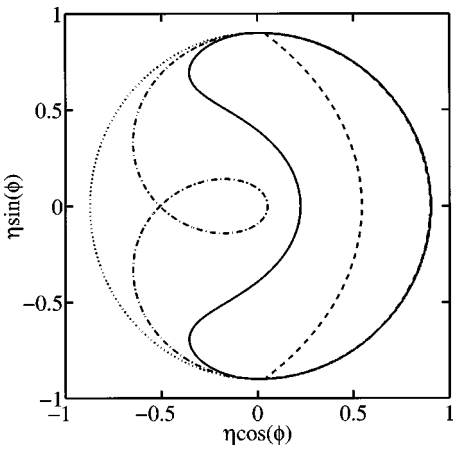

FIG. 5. Phase-plane trajectories for the four-wave mixing process with a signal fraction $\alpha=10\%$: and different normalized mismatches: $\kappa_0=-1$ (dashed curve), $\kappa_0=-0.3258$ (solid curve), $\kappa_o=0.0091$ (dot-dashed curve), $\kappa_o=1$ (dotted curve).

and sideband waves, or a FM eigenmodulation), which exists in the range $-\frac{1}{3}<\kappa_0<\frac{5}{8}$. This mode exists also in the limit of vanishing signal fraction $\alpha=0$ [37], as shown by the dotted line in Fig. 4(a). Finally, the mixed-mode exchange its stability in a secondary bifurcation point $\kappa_0=\frac{5}{8}$ with a pure sideband mode $\eta_e=0$ (which, however has scarce relevance for our problem). Here, the key point is that the unstable FM eigenmodulation, becomes accessible to our injected field for a critical choice of the signal fraction $\alpha=\alpha_c$. The value of α_c is reported as a function of κ_0 in Fig. 4(b). Note that α_c vanishes when we approach the regime described by the linear (undepleted) stability analysis, i.e., for $\kappa_0\rightarrow-\frac{1}{3}$. The critical value of signal fraction α_c turns out to mark a transition between the strong and weak conversion regimes. This is conveniently shown in a phase space $\eta\cos(\phi),\eta\sin(\phi)$ associated with the reduced Hamiltonian system. In this plane, the field evolution along the fiber corresponds to a contour level of the Hamiltonian. The closest this contour level approaches the origin, the strongest the conversion. In Fig. 5, we display different trajectories for a fixed signal level $\alpha=0.1$, and different values of the frequency detunings corresponding to $\kappa_0=-1$ (dashed line), $\kappa_0=-0.3258$ (solid line), $\kappa_0=0.0091$ (dot-dashed line), and $\kappa_0=1$ (dotted line). The nonlinear phase matching ($\kappa_0=-1$), gives a relatively weak achievable conversion (see dashed line). However, the conversion is enhanced (see solid curve) for increasing values of κ_0, entailing a signal detuned on the high-frequency side from the nonlinear phase-matching condition. Importantly, the conversion keeps on increasing even when the signal is detuned outside the linear gain bandwidth (i.e., for $-\frac{1}{3}<\kappa_0$), until the critical condition is reached (dot-dashed curve for $\kappa_0=0.0091$). For this particular input condition the evolution occurs along one branch of the double-loop separatrix, asymptotically toward the FM eigenmodulation represented by the saddle point. A further increase in frequency results into trajectories which move in the outer domain with respect to the separatrix, corresponding to a rapidly dropping conversion. Well above this transition, the trajectories are almost circles, which correspond to a vanishing conversion (see, e.g., the dotted line obtained for $\kappa_0=1$). To show more explicitly that the optimum conversion is obtained outside

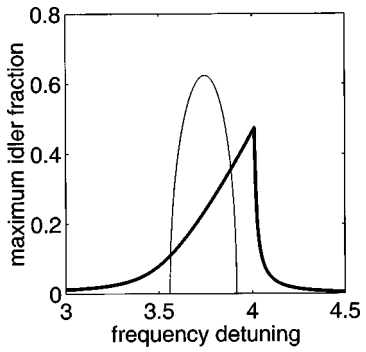

FIG. 6. Maximum achievable idler power fraction as a function of signal frequency detuning Ω for an input signal fraction $\alpha=5\%$ and a walk-off parameter $\delta=2$. Superimposed is the MI gain $g(\Omega)$ obtained with the same value of δ.

the parametric gain bandwidth, in Fig. 6 we display the maximum idler fraction (thick solid curve) generated along the fiber as a function of the signal frequency detuning Ω, as obtained from the solutions of Eqs. (4), for a fixed normalized walk-off δ and signal fraction α. We also display in Fig. 6 the gain $g=g(\Omega)$ obtained with the same value of δ (thin solid curve). Two essential features are immediately clear. (i) In the nonlinear regime, the optimum conversion occurs outside the linear gain bandwidth, with a large factor enhancement ($\simeq 2$) with respect to the signal frequency corresponding to the maximum gain. (ii) The parametric conversion drops abruptly above a critical frequency, due to the separatrix crossing discussed above.

D. Validity of the four-wave truncated model

In this subsection we assess the validity of the four-mode truncation by integrating numerically the ICNLSE model (2). The existence of separatrices and the consequent sensitivity to the input condition would call for a careful choice of the numerical scheme. Nevertheless, we make use of a standard beam propagation (i.e., splitstep) method, whose outcome is shown to be in good quantitative agreement with the predicted dynamics. Let us consider, first, the regime of relatively low power (i.e., $\delta>0.5$). To fix the ideas, we choose a fixed signal input fraction $\alpha=5\%$ and a normalized walk-off $\delta=2$ representative of a power of 40 W in our experiment. Figure 7 shows that for a frequency $\Omega=4.05$ ($\kappa=0.2$), only a weak periodic conversion occurs. However, as expected from the low-dimensional dynamics, only a slight decrease ($\sim 2\%$ in this example) of the signal frequency is sufficient to trigger the interaction into the regime of full periodic conversion, as shown in Fig. 8 for $\Omega=3.95$ ($\kappa=-0.2$). Similarly we have found that the abrupt transition between the two regimes occurs as well for a fixed frequency Ω and a slight change of signal fraction α. As shown in Figs. 7 and 8, the dynamics is actually ruled by the three injected waves and the generated idler, and neither higher-order sidebands, nor the orthogonally polarized Stokes–anti-Stokes pair are appreciably generated. This is no longer true for small enough δ. For instance, let us consider the case $\delta=0.5$ (representative of a power of about 450 W in our experiment). If we set now the modulation frequency at the value $\Omega=0.73$ which corresponds to the full conversion regime of the four-

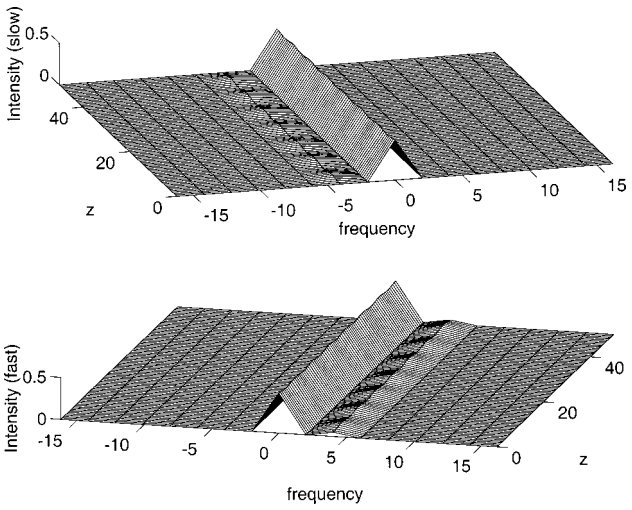

FIG. 7. Evolution of the spectral content of the linearly polarized components ruled by the ICNLSs, as obtained for $\alpha=0.05$ (5% input signal), $\delta=2$ and $\Omega=4.05$ ($\kappa=0.2$). Here the normalized distance is $z=Z/L_{nl}$ and the frequency is the signal detuning $\Omega=2\pi f T_0$.

wave interaction (described by the same value $\kappa=-0.2$ as in Fig. 8), we observe the dynamics shown in Fig. 9. In this case, both the higher-order sidebands and the orthogonally polarized Stokes–anti-Stokes pair are generated, causing the full conversion to be spoiled. It is clear that the additional sideband pair induces a short period dynamics which interferes with the long range dynamics driven by the four-wave interaction. Recalling that δ depends inversely on the optical power, this sets a limitation to the maximum power that can be used to observe the abrupt transition between the two regimes of conversion. Obviously, one has to trade-off between this limitation and the need for a sufficient parametric amplification.

III. EXPERIMENTAL STUDY

In this section we present our setup and experimental results. We compare the spontaneous (i.e., building up from noise) and induced MI or parametric amplification. At the

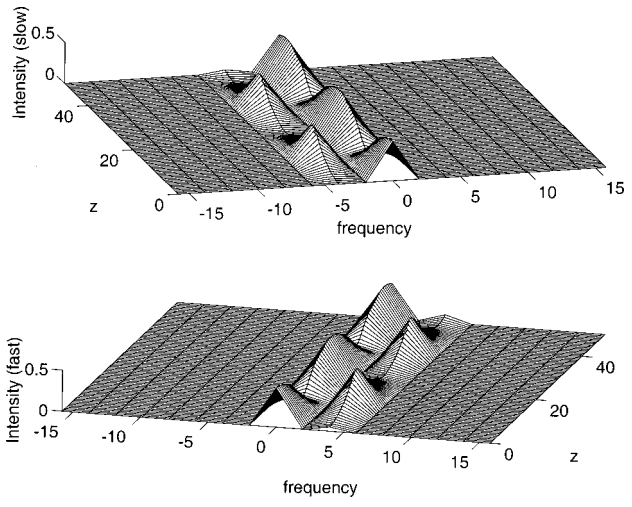

FIG. 8. As in Fig. 7 for $\Omega=3.95$ ($\kappa=-0.2$).

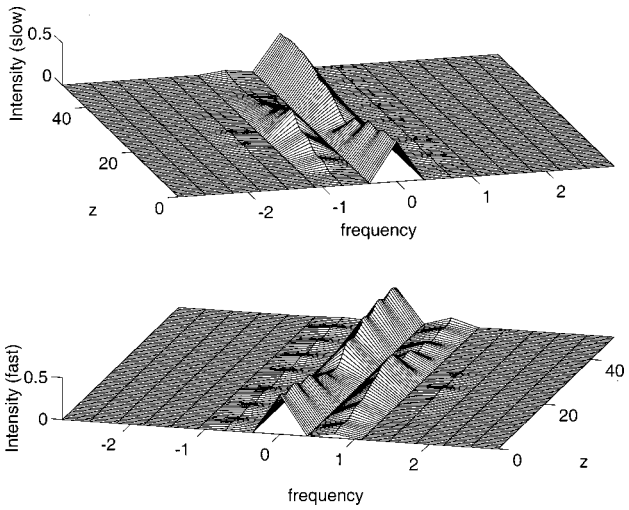

FIG. 9. As in Fig. 7 for $\delta=0.5$ and $\Omega=0.73$ ($\kappa=-0.2$).

power level that we use in the experiment, the parametric amplification of noise occurs with negligible pump depletion. Hence, we assume reasonably that the spectral peak of the parametrically amplified noise is well described by the results of the LSA. Our main focus is to show that, at the same pump power level, when the parametric mixing is seeded by a finite signal wave and pump depletion becomes definitely relevant, the largest conversion is observed at a significant frequency offset from the observed peak of the spontaneous process.

A. Experimental setup

The experimental setup that we have employed for the observation of induced MI in a highly birefringent fiber is shown in Fig. 10. Quasi-cw waves have been obtained by two different laser sources producing nanosecond pulses. With such pulse durations, the two injected waves can be considered as quasi-cw in comparison with the inverse of the frequency detuning (or MI period in the spontantaneous case) which is of the order of a picosecond or less. The pump beam was obtained from a cw tunable ring dye laser, pumped by cw argon laser and amplified by a three-stage dye cell. This dye amplifier was pumped by a frequency-doubled, injection-seeded, and *Q*-switched Nd:YAG laser ($\lambda=532.26$ nm), working with a repetition rate of 25 Hz. The signal pulses were obtained by frequency shifting the Nd:YAG frequency by means of self-stimulated Raman scattering in a multipass carbon dioxide cell. The first Stokes wave, shifted by 41.64 THz from the input laser, was filtered by means of a direct vision prism. The signal and pump pulses were synchronized by sending the pump beam into an optical delay line. We obtained pump and signal beams with proper polarization and adjustable power by employing two laser polarizers and a half-wave plate followed by a set of neutral-density filters. In all our experiments, the pump wavelength was tuned around $\lambda_p=578$ nm whereas the signal wavelength was fixed to $\lambda_s=574.72$ nm. The pump and signal beams were finally combined by a beam splitter, and focused with a $20\times$ microscope objective onto a fiber of fixed length $Z=1.8$ m. The linear parameters of the fiber are known to be a GVD $k''=60\ \mathrm{ps}^2\,\mathrm{km}^{-1}$ (at $\lambda_p=572$ nm) and a

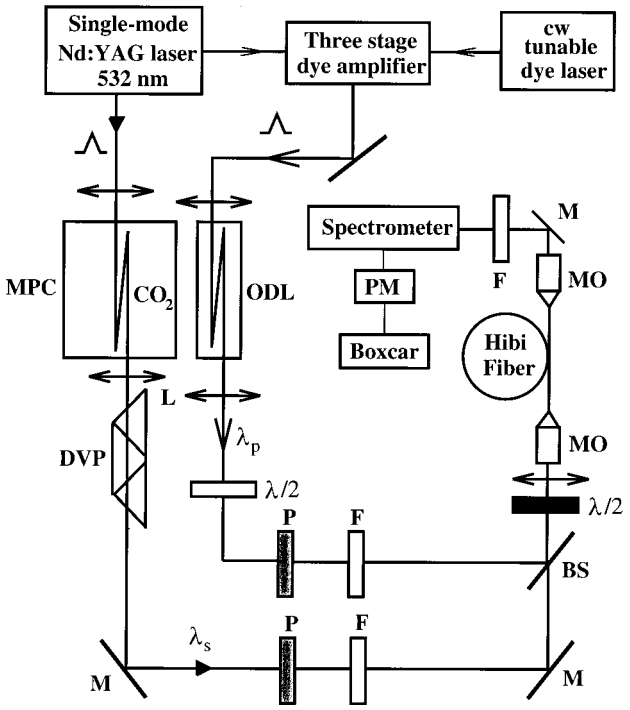

FIG. 10. Shematic diagram of the experimental apparatus. MOs, objective microscope, Fs, neutral filters Ps, Glan-Foucault polarizers, λ/2, half-wave plate, DVP, direct vision prism, MPC, multiple passage cell, ODL, optical delay line, PM, photomultiplier, BSs, beams splitter, Ls, lenses.

group delay $V_x^{-1}-V_y^{-1}=1.17\,\mathrm{ps/m}$, the latter value being confirmed also from nonlinear measurements (see below). The nonlinear coefficient γ was only estimated from measurements of the effective area, while its final value $\gamma=0.05\,\mathrm{W^{-1}\,m^{-1}}$ is obtained from nonlinear measurements as outlined below. The output light has been analyzed by means of a spectrometer with a resolution of 1 $\mathrm{cm^{-1}}$. The signal has been detected by a photomultiplier and sampled and averaged by a boxcar integrator.

B. Experimental results

In a first set of measurements we have injected only the pump beam to record the spectra of parametrically amplified noise. A typical result obtained for $P_{\mathrm{tot}}=P_p=56\,\mathrm{W}$ is shown in Fig. 11. This also allows us to obtain the value of the nonlinear coefficient γ, whose direct estimation based on the effective area could be otherwise affected by a large error. Knowing with good accuracy the other parameters (power, dispersion and group delay), we obtain γ by comparing the measured frequency of the peak amplified noise with the optimum frequency from the LSA. To verify that the frequency of the peak amplified noise depends on power, we have made repeated spectral measurements at several power values up to about 150 W. The results are summarized in Fig. 12. The solid curve is obtained from LSA by adjusting γ to fit the data. These results clearly demonstrate the nonlinear nature of the phase-matching process: the peak MI frequency decreases with power in good agreement with the results of the LSA. For sake of comparison, the dashed line shows how the nonlinear phase-matching frequency obtained from the four-wave model deviates from the observed behavior (as already shown in dimensionless form in Fig. 6). We point out that, at power levels higher than 150 W, the spontaneous MI measurements start to be affected by pump depletion making the comparison with the results of the LSA meaningless (the only way to avoid depletion would be a destructive measurement where the fiber must be cut back as the power is increased so to maintain constant the overall gain).

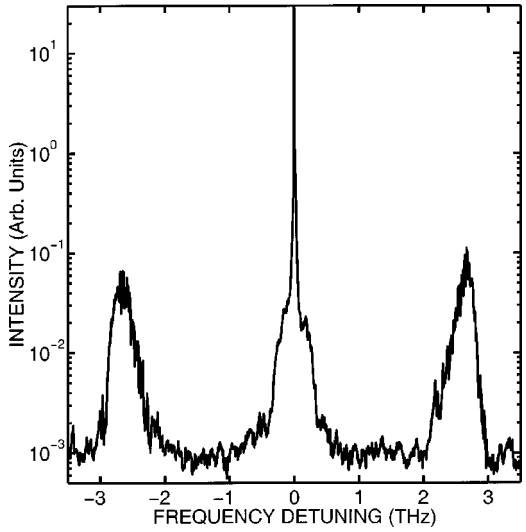

FIG. 11. Spontaneous modulational instability spectrum (i.e., parametrically amplified spontaneous noise), as measured for a fixed total peak power $P_{\mathrm{tot}}=P_x+P_y=56\,\mathrm{W}$.

To test the value of the linear group delay, which is also a key parameter, we have also made a different set of nonlinear measurements of spontaneous MI pumped by a dual wavelength beam (two orthogonally polarized modes at wavelength λ_p and λ_q, respectively). Tuning the wavelength λ_q (i.e., the frequency separation between the pump beams) amounts to change the birefringence. We report in Fig. 13 the optimum detuning measured as a function of λ_q. As in Ref. [21] we find a critical gap where MI is no longer observed [this is due to the existence of a lower bound in δ, see Figs. 1(a) and 1(b)]. Far from the gap the detuning is not appreciably affected by the nonlinearity and hence it permits

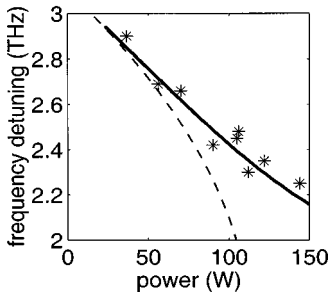

FIG. 12. Measured values of frequency detunings (stars) of the peak spontaneous MI versus total peak power $P_{\mathrm{tot}}=P_x+P_y$. The detunings are obtained from a set of spectra analogous to that of Fig. 11, recorded for different pump powers. The solid line is a theoretical fit obtained from the six-wave LSA with a nonlinear coefficient $\gamma=0.05$. For comparison we report also the four-wave nonlinear phase-matching curve which corresponds to $\kappa=-1$ (dashed line).

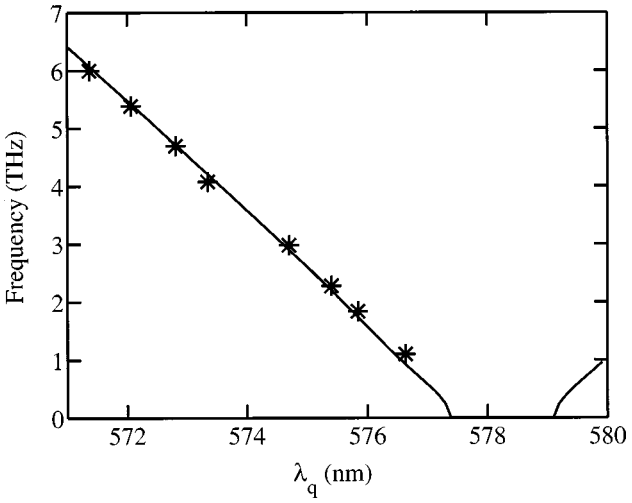

FIG. 13. Frequency detuning of the peak parametrically amplified noise as obtained in a series of experiments with dual-wavelength pumping, where the pump wavelength λ_q on the horizontal axis is tuned across the fixed wavelength $\lambda_p = 574.75$ nm of the other pump beam. The two pump beams have orthogonal polarization along the fiber axes, and a fixed power $P_x = P_y = 20$ W each. The fiber length is $Z = 5$ m.

to extrapolate the value of group delay if the dispersion is known [21]. The results of the LSA (see solid line in Fig. 13) fit the measured values with $V_x^{-1} - V_y^{-1} = 1.17$ ps/m.

A second set of measurements is performed with a finite signal seed. The dependence of the signal-idler conversion is displayed in Fig. 14 which shows a set of experimental power spectra obtained for increasing values of the pump-signal frequency detuning f. These spectra have been recorded with a fixed pump peak power of 56 W (which corresponds to a dimensionless walk-off $\delta = 1.43$), and a fixed signal input power fraction $\alpha = 10\%$. In Fig. 14(a) the spontaneous MI is also clearly seen. In this case the signal was tuned just below the parametric gain bandwidth set by the spontaneous process (see Fig. 11) and the conversion from the pump beam toward the signal-idler pair is weak. As shown in Fig. 14(b), a similar conversion is obtained when we tune the signal frequency close to the value $f = 2.7$ THz which corresponds to the maximum spontaneous MI (i.e., peak of the parametrically amplified noise, see Fig. 11). On the other hand, when we increase f towards the highest bound of the linear gain bandwidth [Figs. 14(c) and 14(d)] the conversion increases until it reaches its maximum for f around 3 THz [Fig. 14(d)]. Notice that, at this signal frequency, the spontaneous process in Fig. 11 shows no appreciable amplification. Above this value, if we keep on increasing f, the conversion decreases very rapidly [see Figs. 14(e) and 14(f)]. Figure 15 compares the measured variation of the generated idler power fraction (stars) with that expected on the basis of the four-wave model (4). The pulsed nature of the waves has been taken into account as explained in detail in Ref. [27]. We also report the theoretical gain curves obtained by the LSA (dashed line). As shown, for a frequency detuning of 3 THz the idler energy reaches its maximum (14%) and in accordance with the Manley-Rowe invariant [$\alpha = (|E_a|^2 - |E_S|^2)/P_{\text{tot}}$], the corresponding signal wave fraction is equal to 24% which amounts to a total frequency

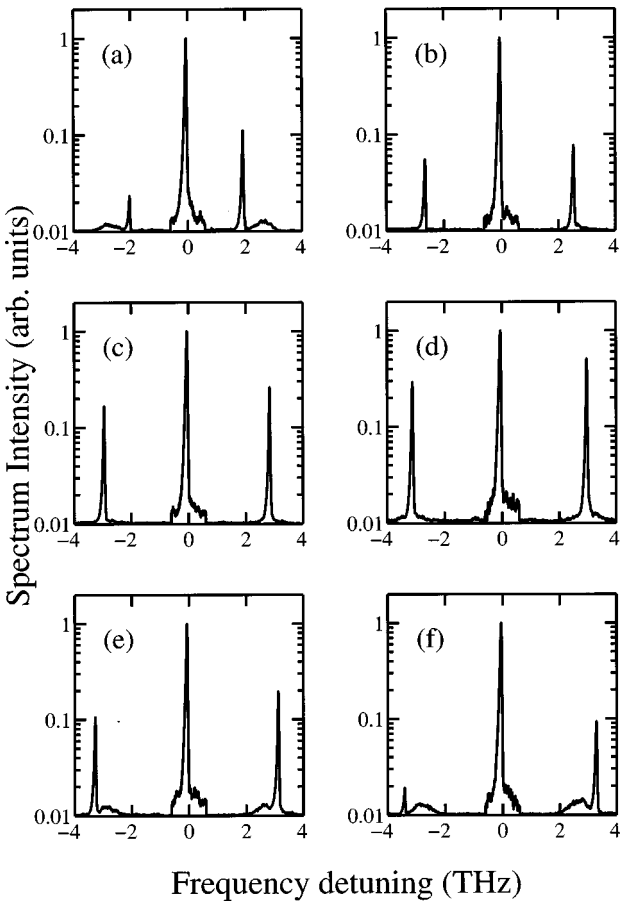

FIG. 14. Output experimental spectra for a total peak pump power of 56 W, and a signal fraction $\alpha = 10\%$: (a) $f = 2.25$ THz, (b) $f = 2.7$ THz, (c) $f = 2.85$ THz, (d) $f = 3$ THz, (e) $f = 3.15$ THz; (f) $f = 3.3$ THz.

conversion of 38%. We emphasize that with such a strong pump depletion, the small signal analysis is unable to reproduce the experimental data, whereas we have a good agreement with the four-wave model conversion curve which fully includes the effect of pump depletion. It is important to note that the optimum frequency conversion is obtained for a frequency detuning which is above the highest bound of the

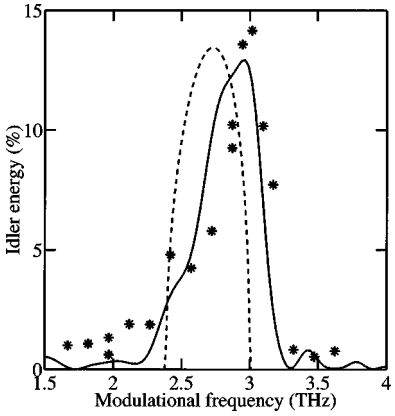

FIG. 15. Experimental (stars) and theoretical (solid curve) idler conversion versus the pump-signal frequency detuning f, with a pump power $P_p = 56$ W, and an input signal fraction $\alpha = 10\%$. Dashed curve, linear MI spectral profile (arbitrary units).

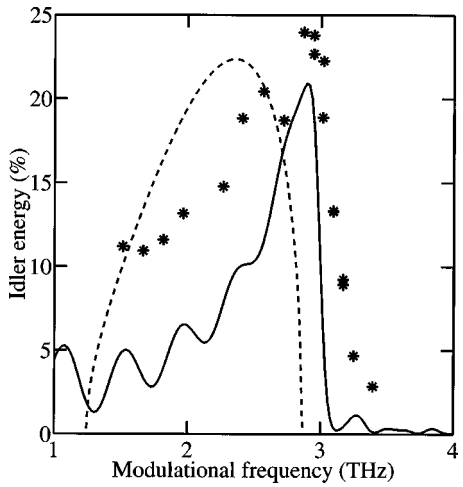

FIG. 16. As in Fig. 15 with a pump power $P_p = 112\,\mathrm{W}$ and $\alpha = 5\%$.

linear gain bandwidth, or in other words for an initially significantly phase-mismatched process. To compare with the strong conversion regime of polarization MI in a weakly birefringent fiber [27,38], in that case we have achieved a more pronounced opposite frequency offset. This is because the nonlinear contribution to the phase mismatch with respect to the birefringent part is less important in highly birefringent fibers than in weakly birefringent fibers. Consequently, the frequency shift is more significant in low birefringence fibers [27,38].

A similar comparison between the experimental conversion measured from induced MI in highly birefringent fibers and the different theoretical models is shown in Fig. 16. All parameters are identical to Fig. 15, except for a total pump peak power and a signal fraction which are now equal to 112 W and 5%, respectively. With this larger pump power, we can see that the difference between the small-signal (undepleted) and large-signal (depleted) model is more pronounced. The frequency shift of the optimum frequency is more relevant (0.6 THz for $P_p = 112\,\mathrm{W}$ against 0.3 THz for $P_p = 56\,\mathrm{W}$) because the total conversion is around 60% for this pump power level. In this case the agreement between the four-wave model and the experimental data is good for modulational frequencies above 2.7 THz. Below this value the experimental conversion is underestimated because for signal frequencies around 2.3 THz (i.e., the nonlinear phase-matching frequency), the signal wave lies in the linear gain bandwith and so we have both the induced and the spontaneous MI. In Fig. 15, for a pump peak power $P_p = 56\,\mathrm{W}$, the spontaneous MI is less important and so we have a better agreement with the experimental data.

IV. CONCLUSIONS

In this paper, we have studied the strongly depleted regime of induced MI in highly birefringent fibers. This nonlinear stage of MI has been theoretically analyzed by use of a four Fourier mode truncation of the coupled nonlinear Schrödinger equations. As in a weakly birefringent fiber, the stability analysis of the system eigenmodes reveal that the maximum achievable conversion was obtained for a signal frequency outside the linear gain bandwidth. We have realised a set of quasi-cw experiments with two different peak powers and we have obtained in both cases a strong frequency conversion from the pump wave towards the first-order sidebands. As expected, with such a strong pump depletion, the optimum conversion is obtained for a frequency detuning which deviates of a significant amount from the prediction of the LSA and the nonlinear phase-matching argument.

APPENDIX: EIGENMODES OF THE FOUR-WAVE INTERACTION

In this appendix, we discuss the existence of the four-wave eigenmodes and their physical accessibility with our experimental conditions (parametric amplification seeded by the anti-Stokes sideband). These eigenmodes, by definition, are those values $(\eta,\phi) = (\eta_e,\phi_e)$ which give vanishing derivatives $d\eta/dz = d\phi/dz = 0$ in Eqs. (10),(11). The analysis closely follows that of Ref. [27], for a low birefringence fiber described by a system analogous to Eqs. (10)–(12). In a Hamiltonian system, the stable eigenmodes are of minor interest since they can be observed only when they are excited at the input, that is, whenever $\eta_0 = \eta_e$, $\phi_0 = \phi_e$, where $\eta_0 = \eta(z=0)$, $\phi_0 = \phi(z=0)$. Conversely, the unstable eigenmodes affect mostly the dynamics, since they can be reached from an entire set of different input conditions η_0,ϕ_0, which evolve asymptotically towards the eigenmode η_e,ϕ_e. In the simplest mechanical analogy, stable and unstable eigenmodes, correspond to the down-rest and up-rest positions of a conventional pendulum, respectively. In the case of the unstable eigenmode excitation, a dramatic output sensitivity to small changes of the input conditions must be expected (in the example, small energy changes induces qualitative changes of the pendulum motion, i.e., a transition from libration to rotation). In our experiment, this means small changes around a critical value of the signal fraction α for a fixed value of frequency and power (i.e., a fixed κ), or small changes in frequency for a fixed α and optical power. This critical input condition is obtained by calculating the eigenmode η_e,ϕ_e from Eqs. (10) and (11), and then by exploiting the invariance of the Hamiltonian between the initial state $H = H_0$ $(\eta_0 = 1-\alpha)$ and the asymptotic state $H = H_e(\eta_e,\phi_e)$, which gives the following equation

$$\underbrace{r\,\eta_e[(1-\eta_e)^2-\alpha^2]^{1/2}\cos\phi_e-(\kappa_0(1-\alpha)-1)\,\eta_e-\eta_e^2}_{H_e(\eta_e,\phi_e,\alpha,\kappa)} = \underbrace{-(\kappa_0(1-\alpha)-1)(1-\alpha)-(1-\alpha)^2}_{H_0(\eta_0=1-\alpha,\phi,\alpha,\kappa)}, \tag{A1}$$

where we have introduced the parameter $\kappa_0 = \Delta k/(\gamma P_p) = \kappa/(1-\alpha)$.

From Eqs. (10) and (11) we find two trivial eigenmodes, which represent the pump mode $\eta_e = 1$ (it exists only in the limit $\alpha = 0$) and the sideband mode $\eta_e = 0$, respectively. Together with the critical value of α obtained from Eq. (A1), their expression reads

$$\eta_e = 1 \begin{cases} \alpha = 0, \quad -\frac{5}{3} < \kappa_0 < -\frac{1}{3}, \\ \phi_e = \cos^{-1}\left[-\frac{3}{2}(\kappa_0 + 1) \right], \end{cases} \tag{A2}$$

$$\eta_e = 0 \begin{cases} \alpha = \frac{\kappa_0}{\kappa_0 + 1}, \quad \frac{5}{8} < \kappa_0 < \infty \\ \phi_e = \cos^{-1}\left(-\frac{3}{2\sqrt{1 + 2\kappa_0}} \right). \end{cases} \tag{A3}$$

These two eigenmodes are unstable over the whole range of κ_o reported above, where the phase ϕ_e is defined. Other two eigenstates are mixed-mode eigenmodulations, either of the AM type ($\phi_e = 0$), or FM type ($\phi_e = \pi$). Only the FM eigenmodulation is unstable and hence accessible with the asymmetric excitation. In this case, by solving Eq. (A1) coupled to the equation $\partial\phi/\partial z|_{(\eta_e, \phi_e)} = 0$ which follows from Eq. (11) with $\cos(\phi_e) = -1$, we obtain that η_e is a real root of a fourth-order polynomial, with the following dependence on κ_0

$$\begin{aligned} p(x) = {} & (405\kappa_0^4 + 2430\kappa_0^3 + 2880\kappa_0^2 + 1800\kappa_0 + 100)x^4 \\ & + (-810\kappa_0^4 - 6480\kappa_0^3 - 10\,530\kappa_0^2 - 9000\kappa_0 - 1800)x^3 \\ & + (-324\kappa_0^4 + 486\kappa_0^3 + 4626\kappa_0^2 + 9090\kappa_0 + 2700)x^2 \\ & + (1296\kappa_0^3 + 1746\kappa_0^2 - 3600\kappa_0 - 1710)x - 1296\kappa_0^2 \\ & + 162\kappa_0 + 405, \end{aligned} \tag{A4}$$

while the critical value of α is obtained in the form

$$\alpha = \frac{q(\eta_e, \kappa_0)}{r(\eta_e, \kappa_0)}, \tag{A5}$$

where $q(\eta_e, \kappa_0)$ and $r(\eta_e, \kappa_0)$ are, respectively, a third and second order polynomial with the following explicit expressions:

$$\begin{aligned} q(\eta_e, \kappa_0) = {} & (90\kappa_0^2 + 225\kappa_0 + 70)\eta_e^3 + (81\kappa_0^3 + 171\kappa_0^2 \\ & - 414\kappa_0 - 205)\eta_e^2 + (-81\kappa_0^3 - 486\kappa_0^2 \\ & + 126\kappa_0 + 180)\eta_e + 225\kappa_0^2 + 63\kappa_0 - 45, \end{aligned} \tag{A6}$$

$$\begin{aligned} r(\eta_e, \kappa_0) = {} & (81\kappa_0^3 + 351\kappa_0^2 + 171\kappa_0 + 70)\eta_e^2 \\ & + (-81\kappa_0^3 - 495\kappa_0^2 - 225\kappa_0 - 45)\eta_e \\ & + 225\kappa_0^2 + 144\kappa_0 + 36. \end{aligned} \tag{A7}$$

These results are summarized in Fig. 4.

ACKNOWLEDGMENTS

The Conseil Régional de Bourgogne, the Center National de la Recherche Scientifique, the Ministère de la Recherche et de la Technologie (Contract ACI Blanche No. 2015), and the Ecole Doctorale Louis Pasteur are gratefully acknowledged for their financial support of this research. S. Trillo acknowledges the kind hospitality from the Laboratoire de Physique de l'Université de Bourgogne.

[1] L. A. Ostroskii, Zh. Eksp. Teor. Fiz. **51**, 1189 (1966) [Sov. Phys. JETP **24**, 797 (1967)].
[2] V. I. Bespalov and V. I. Talanov, Pis'ma Zh. Eksp. Teor. Fiz. **3**, 471 (1966) [JETP Lett. **3**, 307 (1966)].
[3] V. I. Karpman, JETP Lett. **6**, 277 (1967).
[4] T. J. Benjamin and J. E. Feir, J. Fluid Mech. **27**, 417 (1967).
[5] A. Hasegawa and W. F. Brinkman, IEEE J. Quantum Electron. **16**, 694 (1980).
[6] K. Tai, A. Hasegawa, and A. Tomita, Phys. Rev. Lett. **56**, 135 (1986).
[7] K. Tai, A. Tomita, J. L. Jewell, and A. Hasegawa, Appl. Phys. Lett. **49**, 236 (1986).
[8] G. P. Agrawal, *Nonlinear Fiber Optics*, 2nd ed. (Academic, New York, 1995).
[9] A. L. Berkhoer and V. E. Zakharov, Sov. Phys. JETP **31**, 486 (1970).
[10] G. P. Agrawal, Phys. Rev. Lett. **59**, 880 (1987).
[11] S. Wabnitz, Phys. Rev. A **38**, 2018 (1988).
[12] J. E. Rothenberg, Phys. Rev. Lett. **64**, 813 (1990); G. P. Agrawal, *ibid.* **64**, 814 (1990).
[13] J. E. Rothenberg, Phys. Rev. A **42**, 682 (1990).
[14] P. D. Drummond, T. A. B. Kennedy, J. M. Dudley, R. Leonhardt, and J. D. Harvey, Opt. Commun. **78**, 137 (1990).
[15] S. Trillo, and S. Wabnitz, J. Opt. Soc. Am. B **9**, 1061 (1992).
[16] J. E. Rothenberg, Electron. Lett. **28**, 479 (1992).
[17] N. Christensen, R. Leonhardt, and J. D. Harvey, Opt. Commun. **101**, 205 (1993).
[18] R. Leonhardt and J. D. Harvey, IEEE J. Quantum Electron. **30**, 1463 (1994).
[19] E. A. Golovshenko and A. N. Pilipetskii, J. Opt. Soc. Am. B **11**, 92 (1994).
[20] S. G. Murdoch, R. Leonhardt, and J. D. Harvey, Opt. Lett. **20**, 866 (1995).
[21] E. Seve, P. Tchofo-Dinda, G. Millot, M. Remoissenet, J. M. Bilbault, and M. Haelterman, Phys. Rev. A **54**, 3519 (1996); P. Tchofo-Dinda, G. Millot, E. Seve, and M. Haelterman, Opt. Lett. **21**, 1640 (1996).
[22] E. Lantz, D. Gindre, H. Maillotte, and J. Monneret, J. Opt. Soc. Am. B **14**, 116 (1997).
[23] G. Millot, S. Pitois, P. Tchofo-Dinda, and M. Haelterman, Opt. Lett. **22**, 1686 (1997).
[24] S. Trillo, S. Wabnitz, Phys. Rev. E **56**, 1048 (1997).
[25] G. Millot, E. Seve, and S. Wabnitz, Phys. Rev. Lett. **79**, 661 (1997).
[26] G. Millot, E. Seve, S. Wabnitz, and M. Haelterman, J. Opt. Soc. Am. B **15**, 1266 (1998).
[27] G. Millot, E. Seve, S. Wabnitz, and M. Haelterman, Opt. Lett. **23**, 511 (1998).
[28] M. I. Rabinovich and A. L. Fabrikant, Zh. Eksp. Teor. Fiz. **77**, 617 (1979) [Sov. Phys. JETP **50**, 311 (1979)].
[29] E. Infeld, Phys. Rev. Lett. **47**, 717 (1981).
[30] A. M. Kamchatnov, Phys. Rep. **286**, 199 (1997).
[31] G. Cappellini and S. Trillo, J. Opt. Soc. Am. B **8**, 824 (1991).

[32] S. Trillo and S. Wabnitz, Opt. Lett. **16**, 986 (1991).
[33] G. Cappellini and S. Trillo, Opt. Lett. **16**, 895 (1991).
[34] G. Cappellini and S. Trillo, Phys. Rev. A **44**, 7509 (1991).
[35] S. Trillo and S. Wabnitz, Phys. Lett. A **159**, 252 (1991).
[36] C. De Angelis, M. Santagiustina, and S. Trillo, Opt. Lett. **19**, 335 (1994).
[37] C. De Angelis, M. Santagiustina, and S. Trillo, Phys. Rev. A **51**, 774 (1995).
[38] S. Trillo, G. Millot, E. Seve, and S. Wabnitz, Appl. Phys. Lett. **72**, 150 (1998).
[39] G. Millot, E. Seve, S. Wabnitz, and S. Trillo, Phys. Rev. Lett. **80**, 504 (1998).
[40] E. Seve, G. Millot, S. Trillo, and S. Wabnitz, J. Opt. Soc. Am. B **15**, 2537 (1998).
[41] S. G. Murdoch, R. Leonhardt, and J. D. Harvey, J. Opt. Soc. Am. B **14**, 3403 (1997).